International Journal of Disaster Risk Science (2023) 14:280–297
https://doi.org/10.1007/s13753-023-00487-w

www.ijdrs.com
www.springer.com/13753

ARTICLE

Seismic Hazard Analysis of China's Mainland Based on a New Seismicity Model

Weijin Xu[1] · Jian Wu[2] · Mengtan Gao[1]

Accepted: 25 March 2023 / Published online: 12 April 2023

Abstract
Based on the seismic source model in the Fifth Generation Seismic Ground Motion Parameters Zonation Map of China (FGSGMPZMC), a new seismic fault model, the new zonation of seismic risk areas (SRAs), and the estimation of seismicity rates for 2021–2030, this study constructed a new time-dependent seismic source model of China's mainland, and used the probabilistic seismic hazard analysis method to calculate seismic hazard by selecting the ground motion models (GMMs) suitable for seismic sources in China. It also provided the probabilities of China's mainland being affected by earthquakes of modified Mercalli intensity (MMI) VI, VII, VIII, IX, and ≥ X in 2021–2030. The spatial pattern of seismic hazards presented in this article is similar to the pattern of the FGSGMPZMC, but shows more details. The seismic hazards in this study are higher than those in the FGSGMPZMC in the SRAs and fault zones that can produce large earthquakes. This indicates that the seismic source model construction in this study is scientific and reasonable. There are certain similarities between the results in this study and those of Rong et al. (2020) and Feng et al. (2020), but also disparities for specific sites due to differences in seismic source models, seismicity parameters, and GMMs. The results of seismic hazard may serve as parameter input for future seismic risk assessments. The hazard results can also be used as a basis for the formulation of earthquake prevention and mitigation policies for China's mainland.

Keywords China's mainland · New seismicity model · Probabilistic seismic hazard analysis (PSHA) · Seismic fault model · Seismic risk areas

1 Introduction

Probabilistic seismic hazard analysis (PSHA), which is based on seismic source models, ground motion models (GMMs), seismicity parameters, and site conditions (most of the time the site conditions are in the GMMs), uses the probability method to calculate the influence of ground motion at the site. Proposed by Cornell (1968), PSHA is widely used in seismic hazard mapping and seismic hazard analysis across the world. In China, the results of PSHA represent an important basis for seismic hazard mapping, disaster loss assessment, and seismic design of new buildings and the evaluation of existing buildings. In 2015, China officially released the Fifth Generation Seismic Ground Motion Parameters Zonation Map of China (FGSGMPZMC; General Administration of Quality Supervision, Inspection and Quarantine of the People's Republic of China 2015), which was based on the results of PSHA. The seismic zonation map represents long-term seismic hazard levels in the future and can serve as a basis for seismic design of buildings for general purposes (Gao 2015).

Aside from the seismic zonation map, given the non-stationarity of strong earthquakes in China's mainland, the Chinese government also attaches great importance to seismic hazard levels within a short period of time (10 years) in the future (Gao 1996; CERPG 2020), and adopts the hazard levels as the basis for formulating relevant policies. Seismic hazard analysis is essential for seismic risk estimation. Based on the latest research results of seismology and geology, such as the fifth generation seismic source model (FGSSM) (Zhou et al. 2013; Gao et al. 2014), the

✉ Weijin Xu
wjxuwin@163.com

✉ Jian Wu
wujian@eq-cedpc.cn

[1] Institute of Geophysics, China Earthquake Administration, Beijing 100081, China

[2] China Earthquake Disaster Prevention Center, Beijing 100029, China

seismic fault model of Shao et al. (2022), the new seismic risk areas (SRAs), and the latest strong seismicity characteristics analysis of China for 2021–2030 (Shao et al. 2020; Shao et al. 2023), this study constructed a time-dependent seismic source model of China's mainland, used PSHA to calculate peak horizontal ground accelerations (PGA) of multiple exceedance probability levels by adopting appropriate GMMs, and expressed the results in hazard maps. The probability of China's mainland being affected by Mercalli intensity (MMI) VI, VII, VIII, IX, and ≥ X earthquakes in 2021–2030 was estimated. The calculated seismic hazard results can provide input for seismic risk assessment and the formulation of relevant government policies.

In recent years, other studies have calculated the probabilistic seismic hazard in China's mainland. For example, Feng et al. (2020) calculated the seismic hazard in China's mainland and adjacent regions by using spatially-smoothed seismicity model, while Rong et al. (2020) studied the seismic hazard in China based on both spatially-smoothed seismicity model and active fault sources. In this article, we compare the seismic hazard results of this study with those of Rong et al. (2020) and Feng et al. (2020). Such comparison is important for developing a full understanding of seismic hazard in China's mainland.

2 Seismic Zones (Belts) and Seismicity Parameters in China

In China, the calculation of seismicity parameters of seismic source zones has distinctive features in that the studies first calculate *b* values and seismic rates in relatively larger regions with similar seismic structure and seismicity characteristics, which are referred to as seismic zones or seismic belts (Fig. 1). Then seismic rates in seismic zones (belts) are assigned to seismic source zones according to relevant rules (described in detail in Sect. 3). The purpose of this method is to have enough earthquakes to calculate seismicity parameters (Pan et al. 2013) while ensuring the similarity of seismic structure and seismicity characteristics. In this study, we used the seismicity parameters of each seismic zone (belt) in the FGSSM (Zhou et al. 2013; Gao et al. 2014) and the seismicity parameters of each seismic zone in 2021–2030 estimated by Shao et al. (2020). This section briefly introduces the seismic zones (belts) and seismicity parameters in China's mainland and its surrounding areas.

2.1 Introduction of Seismic Zones (Belts)

China's mainland is located on the southeast of the Eurasian plate. Under the combined actions of the Indian, Pacific, and Philippine plates, many large fault belts have formed in the region, such as the Tanlu fault belts in eastern China, Ordos block fault belts in central China, Xiaojiang fault belts, Xianshuihe fault belts, Longmenshan fault belts, Kunlun Mountains fault belts in western China, among others. Large earthquakes are mostly distributed on these large fault belts. Seismotectonics in China is characterized by significant spatial differences, with strong seismicity in the west and weak seismicity in the east. According to the geological tectonic environment and the spatial distribution of seismicity, Shi et al. (1982) and Huan et al. (2002) proposed the concept of seismic zones (belts). Seismic zones (belts) refer to areas with similar characteristics of geological structure

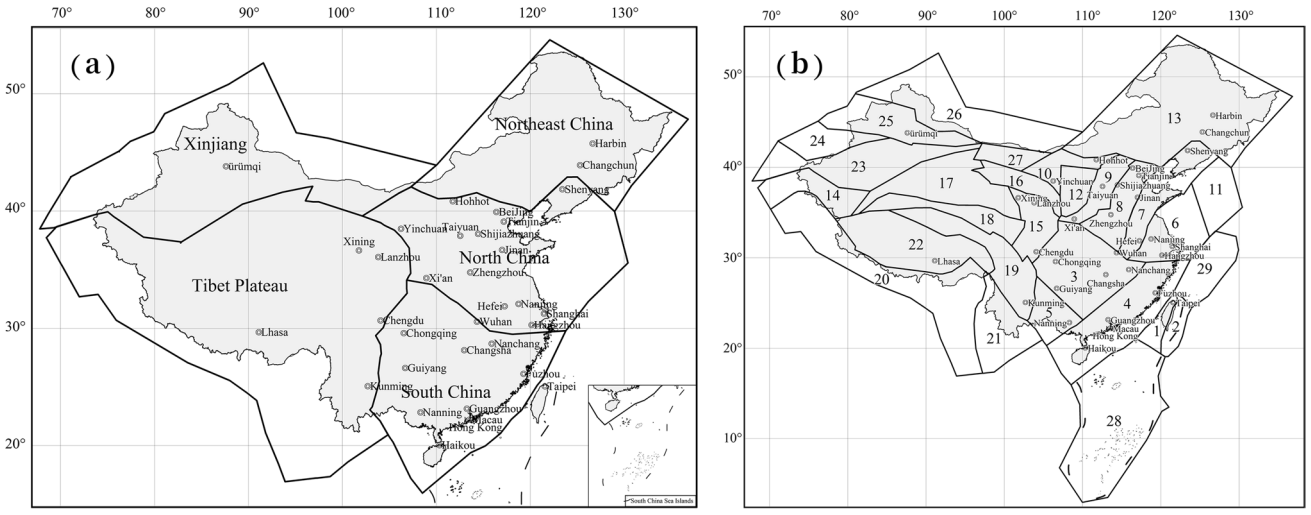

Fig. 1 **a** Division of seismic zones in China's mainland. The black polygons are the seismic zones. There are five seismic zones in China's mainland. **b** Distribution of seismic belts in China. Small black polygons are the 29 seismic belts. The numbers are seismic belt numbers. *Source* WGOSHMII (Working Group II on Seismic Hazard Mapping) (2010)

and seismicity, and represent statistical units for seismicity parameters and for analyzing seismic trends over a certain period in seismic hazard analysis (Shi et al. 1982; Chen et al. 1999; Huan et al. 2002; Pan et al. 2013; Gao 2015). At present, eastern China is divided into the Northeast seismic zone, North China seismic zone, and South China seismic zone, and western China is divided into the Xinjiang seismic zone and Tibet Plateau seismic zone (Fig. 1a). In the FGSSM, Zhou et al. (2013) and Gao et al. (2014) have further divided China's mainland and its surrounding areas into 29 seismic belts (Fig. 1b). These seismic belts constitute the statistical units for seismicity parameter calculation.

2.2 Seismic Rate for Seismic Zones (Belts)

In the FGSSM, the magnitude distribution of seismic activity in seismic zones (belts) conforms to the truncated G–R relationship, and may be written as (Cornell and Vanmarck 1969):

$$\nu(m) = \nu\left(M_0\right)\frac{10^{-b\left(m-M_0\right)} - 10^{-b\left(M_u-M_0\right)}}{1 - 10^{-b\left(M_u-M_0\right)}}, \quad (1)$$

where $\nu(m)$ represents the seismic rate with magnitude greater than or equal to m, $\nu\left(M_0\right)$ is the seismic rate with magnitude greater than or equal to M_0, M_0 is the initial magnitude, M_u is the upper magnitude limit, b is the slope. Pan et al. (2013) calculated the b value and seismic rate of each seismic belt by using the least-square method based on Chinese earthquake catalogs (Table 1). In China, earthquakes with surface-wave magnitude (M_s) 4.0 or above may cause damage, so the initial magnitude selected for calculating seismic rate is M_s 4.0. Pan et al. (2013) used the China earthquake catalogs specifically compiled by Lv et al. (2016) for the FGSGMPZMC. In the earthquake catalogs of Lv et al. (2016), the aftershocks and foreshocks in the catalogs were removed by using the method of Gardner and Knopoff (1974), and the completeness of the catalogue was analyzed according to the degree of linearity of cumulative magnitude–frequency curve. At present, parameters of Pan et al. (2013) have been widely used in the compilation of seismic zonation maps and seismic hazard analysis for engineering sites in China.

In China, strong earthquakes (earthquakes with M_s 6.0 or above in eastern China and M_s 7.0 or above in western China) may cause serious building damage and casualties. The government and policymakers are highly concerned about strong earthquake activities in the near future (next 10 years), with particular attention to whether strong earthquakes will be in an active period, so as to inform short-term earthquake prevention and disaster reduction policies and reduce the impact of earthquake disasters on the society (Gao 1996; CERPG 2020). Shao et al. (2020) and Shao et al. (2023), after analyzing strong earthquake sequences in China's mainland, suggested that currently such earthquakes are in a period of heightened seismicity, and will continue to be so for a period of time in the future (for example, 10 years). The occurrence of large earthquakes in China's mainland fluctuates with time, with large earthquakes relatively frequent in some periods and relatively infrequent in others. Based on the seismic catalogs and paleoearthquakes of Lv et al. (2016), Shao et al. (2020) analyzed the time sequences of large earthquakes, and found that the seismicity level of large earthquakes in China's mainland is relatively high in recent years, and that the seismicity trends of large earthquakes may not change within a short time. Having considered the opinions of other seismologists, Shao et al. (2020) inferred that large earthquakes would maintain the current seismicity level in the next 10 years and employed the Bayesian estimation method to calculate the annual occurrence of strong earthquakes (earthquakes with M_s 6.0 or above in eastern China and M_s 7.0 or above in western China) in the next 10 years in every seismic zone (Fig. 1a). The Tibet Plateau seismic zone excluded the Himalayan arc seismic belt, which had its own calculated rates. The recurrence rates of earthquakes with M_s 6.0 or above in the Northeast China zone, North China zone, and South China zone are 0.11 (recurrence interval 9.1 years), 0.89 (recurrence interval 1.1 years), and 0.29 (recurrence interval 3.4 years) respectively, and the occurrence rates of earthquakes with M_s 7.0 or above in western China and the Himalayan arc are 0.99 (recurrence interval 1.01 years) and 0.20 (recurrence interval 5.0 years), respectively (Shao et al. 2020). The occurrence rates of strong earthquakes estimated by Shao et al. (2020) represent most seismologists' understanding of the spatial–temporal activity of strong earthquakes in China's mainland in the future. At present, the results have been used as the basis for seismic hazard and risk analysis.

In our study, the results of Shao et al. (2020) were used for the seismic rates of strong earthquakes (earthquakes above M_s 6.0 in eastern China and above M_s 7.0 in western China). For earthquakes with M_s 6.0 or below in eastern China and M_s 7.0 or below in western China, the time-independent seismic rates calculated by Pan et al. (2013) for the FGSSM were adopted. We first calculated the seismic rates of strong earthquakes in each seismic belt (column 7 in Table 1) based on the doubly truncated exponential magnitude–frequency model of Cornell and Vanmarck (1969) and the parameters of Pan et al. (2013) (columns 4, 5, and 6 in Table 1), and then used them as weights to assign the seismic rates of Shao et al. (2020) to

Table 1 Seismicity parameters for the seismic belts of China

Eastern China							
Seismic zones	No.	Seismic belts	Parameters in FGSSM				This study
			M_u	b	ν_4	ν_6	ν_6
Taiwan	1	Western Taiwan seismic belt	7.5	0.90	22	3.3E−01	3.3E−01
	2	Eastern Taiwan seismic belt	8.0	0.92	107	1.5E+00	1.5E+00
South China	3	Seismic belt in the middle reaches of the Yangtze River	7.0	1.20	3.2	1.2E−02	2.7E−02
	4	South China coast seismic belt	8.0	0.87	5.6	1.0E−01	2.2E−01
	5	Youjiang River seismic belt	7.0	1.04	2.5	1.9E−02	4.2E−02
North China	6	Lower reaches of the Yangtze River–South Yellow Sea seismic belt	7.5	0.85	3.0	5.7E−02	1.3E−01
	7	Tanlu seismic belt	8.5	0.85	4.0	7.9E−02	1.9E−01
	8	North China Plain seismic belt	8.0	0.86	4.6	8.6E−02	2.0E−01
	9	Fenwei seismic belt	8.5	0.78	2.5	6.8E−02	1.6E−01
	10	Yinchuan–Hetao seismic belt	8.0	0.90	4.5	7.0E−02	1.7E−01
	11	North Korea seismic belt	7.0	1.05	2.0	1.4E−02	3.3E−02
	12	Ordos seismic belt	6.5	1.20	1.0	3.0E−03	7.1E−03
Northeast China	13	Northeast China seismic belt	7.5	1.00	5.0	4.8E−02	1.1E−01
–	28	South China Sea seismic belt	7.5	1.05	6.0	4.6E−02	4.6E−02
–	29	East China Sea seismic belt	7.0	1.05	6.0	4.3E−02	4.3E−02
Western China							
Seismic zones	No.	Seismic belts	Parameters in FGSSM				This study
			M_u	b	ν_4	ν_7	ν_7
Tibetan Plateau	14	West Kunlun–Pamir seismic belt	8.0	0.92	50	7.6E−02	1.1E−01
	15	Longmenshan seismic belt	8.0	0.71	5.2	3.1E−02	4.6E−02
	16	Liupan–Qilian Mountains seismic belt	8.5	0.75	6.4	3.3E−02	4.9E−02
	17	Qaidam–Altun seismic belt	8.5	0.84	12	3.4E−02	5.1E−02
	18	Bayan Har seismic belt	8.5	0.75	6.5	3.4E−02	5.1E−02
	19	Xianshuihe–East Yunnan seismic belt	8.0	0.85	34	7.7E−02	1.2E−01
	20	Himalayas seismic belt	9.0	0.86	81	1.8E−01	2.0E−01
	21	Southwest Yunnan seismic belt	8.0	0.77	20	8.1E−02	2.7E−01
	22	Central Tibet seismic belt	8.5	0.81	25	8.7E−02	1.3E−01
Xinjiang	23	South Tianshan seismic belt	8.5	1.1	44	2.2E−02	3.3E−02
	24	Middle Tianshan seismic belt	8.5	0.80	7.0	2.6E−02	3.9E−02
	25	North Tianshan seismic belt	8.0	0.83	9.0	2.5E−02	3.7E−02
	26	Altai seismic belt	8.5	0.75	7.0	3.6E−02	5.4E−02
	27	Tarim–Alashan seismic belt	7.0	1.2	1.6	0.0E+00	0.0E+00

FGSSM fifth generation seismic source model, M_u upper limit magnitude, b value in G–R relationship, ν_4 seismic rate of $M_s \geq 4$, ν_6 seismic rate of $M_s \geq 6$, ν_7 seismic rate of $M_s \geq 7$

the corresponding seismic belts (column 8 in Table 1). The calculation formula is as follows:

$$\nu_{\text{new}} = \frac{\nu_{\text{SB, Pan et al. (2013)}}}{\nu_{\text{SZ, Pan et al. (2013)}}} \nu_{\text{SZ, Shao et al. (2020)}}, \quad (2)$$

where ν_{new} is the new seismic rates of strong earthquakes in the seismic belts, $\nu_{\text{SB, Pan et al. (2013)}}$ is the seismic rates of strong earthquakes in the seismic belts of Pan et al. (2013), $\nu_{\text{SZ, Pan et al. (2013)}}$ is the seismic rates of strong earthquakes in the seismic zones of Pan et al. (2013), and $\nu_{\text{SZ, Shao et al. (2020)}}$ is the seismic rates of strong earthquakes in the seismic zones of Shao et al. (2020). The purpose is to facilitate the application of the parameters of Shao et al. (2020) to seismic hazard calculation in the seismic source zones (described in detail in Sect. 3).

3 Seismic Source Models and Seismicity Parameters

Having explained the earthquake recurrence rates in each seismic belt (zone), in this section we explain how to assign recurrence rates in each belt (zone) to each seismic source zone. In this study, three seismic source model schemes were used for the spatial allocation of earthquake occurrence rates, that is, the FGSSM, seismic fault model, and SRA model. In seismic hazard calculation, the three seismic source model schemes were weighted and summed using the weights of 0.4, 0.4, and 0.2, respectively, to obtain the final exceedance probability. Model 1 is the FGSSM, which was used in compiling the FGSGMPZMC, and is the most widely used seismic source model in China at present. Model 2 is a characteristic fault model, which is one of the main highlights of this article. Compared with area source model, fault model can reflect more near-field motion characteristics. Therefore, models 1 and 2 play a major role in calculating seismic hazard, and each model was assigned a weight of 0.4. Model 3 is a SRA model. Given that the division of SRA has strong subjectivity, it is assigned a lower weight of 0.2. The three models are briefly introduced in the following.

3.1 Model 1: Fifth Generation Seismic Source Model

An important component of this study is the FGSSM. In the FGSSM, the seismic source zones are area sources, comprising areas with the potential to generate damaging earthquakes (Zhou et al. 2013).

The delineation of seismic source zones in China has distinctive features. Considering the spatial heterogeneity of seismotectonics and seismicity in China, Huan et al. (2002) and Zhou et al. (2013) proposed a three-level zoning scheme for seismic sources. This means that the determination of seismic source requires three steps. First, seismic belts are determined according to the consistency of seismicity, geology, seismotectonics, and geotectonics while considering the adequacy of statistical samples in the earthquake catalog (Pan et al. 2013; Zhou et al. 2013; Gao et al. 2014). Seismic belts are also statistical units of seismicity parameters (including seismic rate and *b* value in the Gutenberg–Richter relationship). Second, seismotectonic zones are determined within the seismic belts. Seismotectonic zones are areas demonstrating consistency in seismogenic tectonic model and seismotectonics under the current geodynamic environment (Zhou et al. 2013; Gao et al. 2014). Seismotectonic zones largely reflect the difference in background seismicity in seismic belts, thus are also called background seismic sources. They also reflect the spatial differences of seismogenic tectonic models within the seismic belt (Zhou et al. 2013; Gao et al. 2014). Finally, seismic source zones are determined according to more detailed seismic, geological, and tectonic data in each seismotectonic zone (Zhou et al. 2013; Gao et al. 2014).

In the FGSSM, seismologists in China identified new seismic belts (Fig. 1) and seismic source zones (Fig. 2) according to the above methods, with the whole country divided into 29 seismic belts and 1643 seismic source zones (Zhou et al. 2013; Gao et al. 2014; Gao 2015).

Seismicity parameters mainly include seismic rate, *b* value in the Gutenberg–Richter relationship, and upper magnitude limit (Table 1). The recurrence rate and the *b* value are obtained by the least-square method based on seismic catalog, while the upper limit of magnitude is determined based on geological fault conditions and historical seismicity (Pan et al. 2013). In China, the seismic rate in each seismic source zone is not calculated directly. Instead, the seismic rate and the *b* value are calculated first in the seismic belt (zone), and then the seismic rate is assigned to the seismic source zones within the seismic belt according to the spatial distribution function. The spatial distribution function represents the proportion of the annual seismic rate in the source to the seismic rate in the belt. It is obtained through comprehensive evaluation based on seismicity characteristics, seismotectonic characteristics, and other information (Gao 2015). For a seismic source zone in a seismic belt, the rate of m_i magnitude bin can be calculated using Eq. 3:

$$\nu_{m_i} = f_{m_i} \cdot \nu_{\mathrm{SB,m_i}}, \tag{3}$$

where f_{m_i} is the spatial distribution function of the m_i magnitude bin of the seismic source, it is a known parameter. $\nu_{\mathrm{SB,m_i}}$ is the rate of m_i magnitude bin in the seismic belt. Detailed information on seismic belts, seismic sources, and their seismicity parameters, can be found in the *Handbook of Seismic Ground Motion Parameter Zonation Map of China* (Gao 2015) or publications such as Pan et al. (2013), Xu et al. (2021), and Li et al. (2022).

In this study, we updated the seismic rate of $M_s \geq 6.0$ events in the FGSSM based on the new findings of Shao et al. (2020) (Table 1, column 8) (described in detail in Sect. 2.2). Except for the recurrence rate, other seismicity parameters of sources were consistent with those of the FGSSM, including seismic source boundary, *b* value, and upper limit magnitude.

3.2 Model 2: Seismic Fault Model

Compared with the FGSSM, a major feature of this study is the use of seismic fault model. A large number of earthquake faults are present in China, but many seismogenic

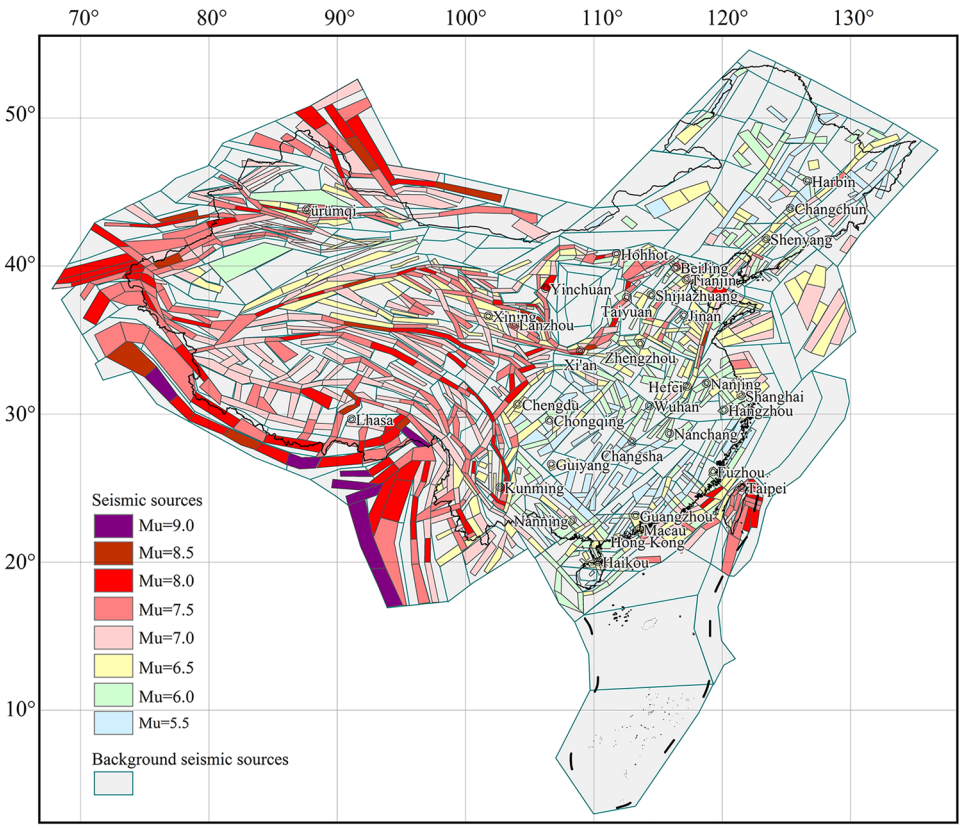

Fig. 2 Distribution of the fifth generation seismic source model in China and adjacent areas. *Source* WGOSHMII (2010). M_u upper limit magnitude of the seismic source

faults remain to be studied in depth, with large uncertainties about their locations, strike, dip direction, and dip angle. Therefore, relevant studies have always used area seismic sources in the seismic source model in China (Gao 2003; Pan et al. 2013; Zhou et al. 2013). In recent years, increased research by geologists on seismogenic faults that can produce large earthquakes has generated abundant data (Zhou et al. 2003; Wen et al. 2007; Xie et al. 2013; Wu et al. 2014; Zheng et al. 2019). This study attempted to use the fault model to improve the accuracy of the seismic source model.

Large earthquakes ($M_s > 6.0$) in China are mainly distributed in large active fault zones (Zhang 1999; Huan et al. 2002; Deng et al. 2003; Shao et al. 2008; Wu et al. 2014; Zheng et al. 2019). Based on the geological and tectonic environment and seismicity characteristics, geologists have established the active block theory, which holds that large earthquakes in China are controlled by the movement and deformation of active blocks, and the epicenters of strong earthquakes are located in the boundary zones of active blocks (Deng 1996; Ma 1999; Deng et al. 2002; Zhang et al. 2003; Zhang et al. 2004). The large earthquakes produced by active faults have resulted in serious disasters (Zhang et al. 2013).

The determination of each stage of large earthquake preparation represents a primary focus in the research on the kinematic process of the in situ recurrence of continental strong earthquakes. Whether the target fault is in the late period of the seismic cycle also constitutes an important background for the prediction of strong earthquake occurrence time. Despite many scientific conundrums in short-term and impending earthquake prediction, in recent years, some studies on large earthquakes around the world show that if the time scale requirements for prediction are relaxed, certain methods can be used to determine the late period in the intervals between large earthquakes (Wang et al. 2019; Shao et al. 2022; Shao et al. 2023). Shao et al. (2022) and Shao et al. (2023) focused on 391 fault segments in the boundary zone of active blocks in China's mainland (Fig. 3), having completed large amounts of field measurements, literature analysis, and calculation. Using an integrative approach combining seismotectonic analysis of unbroken active faults, locking of fault segments from geodesy, definition of fault segments with sparse small and medium magnitude earthquakes, and numerical simulation of Coulomb stress enhancement on some segments, Shao et al. (2022) and Shao et al. (2023) determined the seismic risk of the main fault segments in the boundary zone of continental active blocks in China, and provided the corresponding hazard coefficient to determine which fault segments may be in the late period between earthquakes. The value of hazard coefficient is between 0 and 10, and the greater the coefficient, the higher the hazard (CERPG 2020; Shao et al. 2022). Nearly 30% of

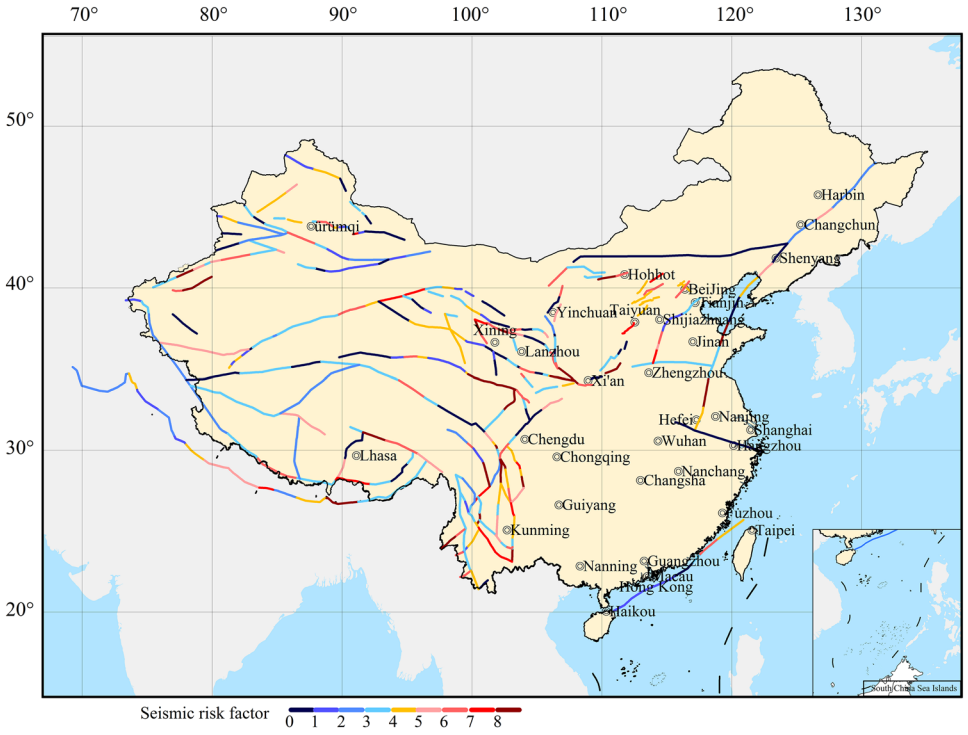

Fig. 3 Seismogenic fault model for China's mainland (including 391 fault segments; the redder the fault segment, the greater the hazard coefficient, and the bluer the color, the smaller the hazard coefficient). *Source* data from Shao et al. (2022)

the 391 fault segments have a hazard coefficient greater than 5 (Fig. 3), which demonstrates the seismic hazard level of major faults in China from a macroscopic perspective. The seismic hazard results calculated using this seismic source model can show more details of hazard spatial distribution than that in FGSGMPZMC.

In this scheme, the faults considered are capable of generating earthquakes with M_s 6.0 and greater (M_s 6.0 in eastern China and M_s 7.0 in western China). Wang et al. (2019) and Wang et al. (2022) estimated the characteristic earthquake return period of each fault based on the multidisciplinary physical observations data, such as paleoearthquakes, fault slip rate, crustal deformation, and so on. According to the aforementioned return period of characteristic earthquakes on faults and its uncertainties, as well as the earthquake elapse time T_e, we calculated the earthquake occurrence probability P in 2021–2030 ($\Delta T = 10$) by using the equation proposed by Matthews et al. (2002) based on the Brownian passage time (BPT) model.

$$P\left(\Delta T|T_e\right) = \frac{\int_{T_e}^{T_e+\Delta T} f(t)\mathrm{d}t}{\int_{T_e}^{\infty} f(t)\mathrm{d}t} = \frac{F\left(T_e+\Delta T\right) - F\left(T_e\right)}{1 - F\left(T_e\right)}. \quad (4)$$

In Eq. 4, $F\left(T_e\right) = \int_0^{T_e} f(t)\mathrm{d}t$ is the cumulative probability distribution function, $f(t) = \sqrt{\frac{\mu}{2\pi\alpha^2 t^3}} \exp\left(-\frac{(t-\mu)^2}{2\alpha^2\mu t}\right)$ is the probability density function of the BPT model, μ is the mean value of earthquake recurrence period, $\alpha = \sigma/\mu$ is the coefficient of variation, and σ is the standard deviation (the occurrence time of the latest earthquake is unknown on some faults, while historical open intervals are known on some faults). In the event of unknown elapsed time of earthquakes on the faults, we used the method proposed by Field and Jordan (2015) to calculate the probability of earthquakes in the future. The random uncertainty of characteristic earthquake return period is also called variation coefficient α, which is the ratio of standard deviation to expected value. If $\alpha = 0$, then the earthquake recurrence is periodic, and if $\alpha = 1$, then the earthquake recurrence is considered to follow the Poisson process. It is very difficult to calculate the variation coefficient, as it is difficult to have sufficient earthquake events on a fault. Internationally, the α value used by researchers is between 0.2 and 0.7 (Cramer et al. 2000). Zöller (2018) believes that the variation coefficient is related to the level of moderate and small events in the study area, and provides the equation for the relationship between variation coefficient and the b value in the G–R relationship:$\alpha = \sqrt{b/(3-b)}$. However, the variation coefficient calculated according to this equation is larger than that adopted by other studies—for example, if $b = 0.7$, then $\alpha = 0.55$, if $b = 1$, then $\alpha = 0.71$. In this study, we comprehensively considered the value calculated based on the equation and the value adopted by studies mentioned above. In addition, we also considered the situation in China, that is, a smaller b value in western China and a higher one in eastern China, by setting $\alpha = 0.6$ in eastern China and $\alpha = 0.5$ in western China.

We then used the formula $r = -\ln(1-P)/\Delta T$ (Petersen et al. 2007) to convert the earthquake occurrence probability to the effective earthquake recurrence rate, which can be used to calculate seismic hazards.

3.3 Model 3: The Model of Seismic Risk Areas

In this study, we also developed a seismic source model based on the SRAs from 2021 to 2030, to highlight the spatial distribution characteristics of earthquakes in China's mainland in this time period. SRAs are areas with relatively high probability of strong earthquakes in the next decade, and represent an important basis for the Chinese government to formulate earthquake emergency preparedness policies (CERPG 2020). All strong earthquakes are expected to occur in the SRAs in the near future (next 10 years), although this is not possible in the real world. Still, future earthquakes are more likely to occur in these areas and their peripheries. Shao et al. (2020) and Shao et al. (2023), based on the activity level of fault segments, and referring to data such as geological structure characteristics and regional fault deformation characteristics, have investigated the area most prone to significant earthquakes in the future, and determined a total of 40 SRAs in China's mainland from 2021 to 2030 (Fig. 4), accounting for about 10% of the area of the region (Shao et al. 2020). Table 2 presents the names corresponding to the codes of SRAs in Fig. 4. The SRAs were determined through a comprehensive seismic and geological analysis, and supplemented by expert judgment.

According to this scheme, strong earthquakes ($M_s \geq 6.0$ earthquakes in eastern China and $M_s \geq 7.0$ earthquakes in western China) will occur in the SRAs in the next 10 years. We assigned the seismic rate in the seismic zones introduced in Sect. 2.2 to each SRA by taking the area of the SRAs as the weights (Table 2). To express the spatial uncertainty of these SRAs, we used the Gaussian spatial smoothing method proposed by Frankel (1995) to extend the SRAs, adopting a Gaussian smoothing kernel with a correlation distance of 50 km. The magnitude–frequency model and upper limit magnitude in the SRAs were consistent with the FGSSM where the SRAs were located (Table 2).

Note that we have focused primarily on the seismic source models and seismicity parameters of $M_s \geq 6.0$ earthquakes in eastern China and $M_s \geq 7.0$ earthquakes in western China. For the seismic source zones of $M_s < 6.0$ earthquakes in eastern China and $M_s < 7.0$ earthquakes in western China, we adopted entirely the seismic source model and seismicity parameters scheme in FGSSM, including the seismic source zone boundary, b value, and earthquake occurrence rate. Different seismic source models were used for earthquakes.

4 Selection of Ground Motion Models (GMMs)

GMMs represent important input for the PSHA. Much research has been done on GMMs, resulting in a large number of GMMs, the most common of which is the five GMMs presented by the NGA-West 2 project (Bozorgnia et al. 2014).

Fig. 4 Key seismic risk areas (encircled by red boundary) in China's mainland. *Source* data from Shao et al. (2020)

Table 2 Seismicity parameters in the seismic risk areas of China's mainland

Seismic risk areas in western China				
Code	Name	ν_7	M_u	b
1	Northwestern segment of the West Kunlun fault area	3.7E−02	8.0	0.92
2	Western segment of the South Tianshan fault area	4.0E−02	8.5	1.10
3	Middle segment of the South Tianshan fault area	3.7E−02	8.5	1.10
4	Middle segment of the North Tianshan fault area	5.1E−02	8.0	0.83
5	Fukang fault area	1.4E−02	8.0	0.83
6	Darbut fault area	1.8E−02	8.0	0.83
7	Eastern margin of Pamir–West Kunlun fault	7.5E−02	8.0	0.92
8	Fenghuoshan Mountain–Yushu Dangjiang segment	4.4E−02	8.0	0.85
9	Bangong Nujiang–Dangyayongcuo north segment	3.2E−02	8.5	0.81
10	Western segment of Jiali fault–eastern segment of Bangong Nujiang River	3.1E−02	8.5	0.81
11	Eastern segment of Jiali fault–Motuo fault	4.9E−02	9.0	0.85
12	Middle-western segment of Himalayan main fault	1.2E−01	9.0	0.85
13	Middle-eastern segment of Himalayan main fault and Lunan segment of Yadong Valley	8.3E−02	9.0	0.85
14	Eastern segment of the Altun fault area	1.7E−01	8.5	0.84
15	Middle segment of the Altun fault area	1.6E−02	8.5	0.84
16	Xidatan–Dongdatan segment of the East Kunlun fault area	1.5E−02	8.5	0.75
17	Middle-western segment of the Qilian fault area	3.2E−02	8.5	0.75
18	Middle-eastern segment of the Qilian fault area	1.0E−02	8.5	0.75
19	Middle-western segment of the West Qinling fault area	2.2E−02	8.0	0.71
20	Eastern segment of the East Kunlun fault area–middle-northern segment of the Longriba fault area	6.5E−02	8.5	0.75
21	Middle-southern segment of the Xianshuihe fault area–southern segment of the Longmenshan fault area	2.2E−02	8.0	0.71
22	Shawan segment of the Litang fault area–Lijiang–Xiaojinhe fault area	2.5E−02	8.0	0.85
23	Anninghe fault area–Daliangshan fault area–Lianfeng and Zhaotong fault areas–middle segment of the Mabian fault area–northern segment of the Xiaojiang fault area	7.0E−02	8.0	0.85
24	Lancang–Longling fault area	7.3E−02	8.0	0.77
25	Chuxiong–Jianshui fault area–Honghe fault area	3.0E−02	8.0	0.85
26	Southern segment of the Xiaojiang fault area–southeastern segment of the Honghe fault area	1.5E−02	8.0	0.85
Seismic risk areas in eastern China				
Code	Name	ν_6	M_u	b
27	Northwestern margin fault area of Ordos	1.2E−01	8.0	0.90
28	Southeastern segment of the Xiangshan–Tianjingshan fault area–Lingwu segment of the Yellow River fault area	6.3E−02	8.0	0.90
29	Southern segment of the Liupanshan fault area–eastern segment of the West Qinling fault area	9.4E−02	8.5	0.78
30	Middle-eastern segment of the Hetao fault area	7.6E−02	8.0	0.90
31	Western segment of the Yanshan fault area–northern segment of the Shanxi fault area	1.5E−01	8.5	0.78
32	Middle segment of the Shanxi fault area	2.1E−02	8.5	0.78
33	Southern segment of the Shanxi fault area	6.9E−02	8.5	0.78
34	Cixian–Hebi segment of the Hebei plain belt	6.1E−02	8.0	0.86
35	Shulan–Wuchang segment of the Tanlu fault area	1.1E−01	7.5	1.00
36	Liaodong segment of the Tanlu fault area	1.1E−01	8.5	0.85
37	Laizhou Bay segment of the Tanlu fault area	5.7E−02	8.5	0.85
38	Suqian–Sihong segment of the Tanlu fault area	6.7E−02	8.5	0.85
39	Changle–Nan'ao fault area	1.5E−01	8.0	0.87
40	Guangdong–Guangxi–Hainan border area	1.4E−01	8.0	0.87

However, some countries and regions also have their specific suitable GMMs. Two sets of GMMs developed by Yu et al. (2013) and Xiao (2011) were selected in this study. The models of Yu et al. (2013) and Xiao (2011) were specially established for seismic hazard analysis in China. They adopt the ground motion records of global earthquakes to develop the GMMs based on a projection method, while continuously updating its coefficients according to the latest ground motion records. The method proposed by Hu and Zhang (1984) was used to project strong ground motion records from other regions to China's mainland, thus solving the problem of the lack of strong ground motion records in the region. See Hong and Feng (2019) for a detailed introduction about this projection method.

The GMMs of Yu (2013) and Xiao (2011) are officially recognized in China. These works considered the consistency between the GMMs and the seismic source zone when compiling the FGSGMPZMC, and the seismic hazard calculated based on the two can best reflect the distribution characteristics of seismic hazard in China's mainland. At present, the two GMMs have been applied to the compilation of China's seismic hazard map, seismic hazard analysis of major projects, and China's earthquake catastrophe model, with their applicability and reliability fully verified. The GMM of Yu et al. (2013) is applicable to area seismic sources zone (models 1 and 3), and the GMM of Xiao (2011) is applicable to fault sources (model 2).

5 Calculation Method of Seismic Hazard

In the calculation of seismic hazard, the seismic source zones were manipulated in several ways: we divided zone area sources into 0.05° × 0.05° grids, and calculated the annual earthquake occurrence rate of each magnitude in each grid. For the fault sources, the fault width was calculated using the empirical relationship of Wells and Coppersmith (1994). The range of the fault projection plane was obtained according to the strike, length, and width of the fault. In actual calculation, these grids and fault projection planes can be regarded as single sources, with no need for further division.

The method used in this study was the classical PSHA method proposed by Cornell (1968). This method is widely used in seismic hazard calculation and seismic hazard mapping in China, the United States, and other countries (Gao 2015; Petersen et al. 2015). The hazard of all seismic sources relevant to the site can be calculated by Eq. 5:

$$\lambda\ (A > a) = \sum_i n_i\left(M_0\right) \int_{m_0}^{M_u} \int_R P(A > a|M,\ R) p_i(M) p_i(R) \mathrm{d}R\mathrm{d}M, \tag{5}$$

where $\lambda\ (A > a)$ is the exceedance probability of seismic hazard, that is, the probability that the ground motion A generated by a potentially damaging earthquake exceeds the ground motion of a given a. $n_i\left(M_0\right)$ is the annual occurrence rate of earthquakes in the ith seismic source with magnitudes greater than or equal to M_0. M_0 is the threshold magnitude. It is generally believed that an earthquake with a magnitude of $M > M_0$ may cause damage to a given site, and M_0 is set as M_s 4.0 in China. $p_i(M)$ is the probability density function of magnitude, which is derived from the magnitude–frequency relation $\ln N(M) = a - bM$ (Gutenberg and Richter 1944). $p_i(R)$ is the probability density function of distance. $P\ (A > a|M,\ R)$ in the seismic hazard calculation equation calculates the probability that the ground motion generated by the earthquake will exceed a given value (Fig. 5a). In the real world, $P\ \left(a_1 < A < a_2|M,\ R\right)$, the probability that the ground motion generated by the earthquake will occur within a certain interval (corresponding to an MMI unit) is also required in the calculation process (Fig. 5b). At present, as a general practice in China, the calculation of exceedance probability is realized by centralized correction of ground motion uncertainties of all sources in the last step, thus able to obtain only the probability of ground motions exceeding a given value, but not the probability of ground motions occurring within a certain interval. In this study, we improved the algorithm of seismic hazard calculation to enable the calculation of the probability of ground motion

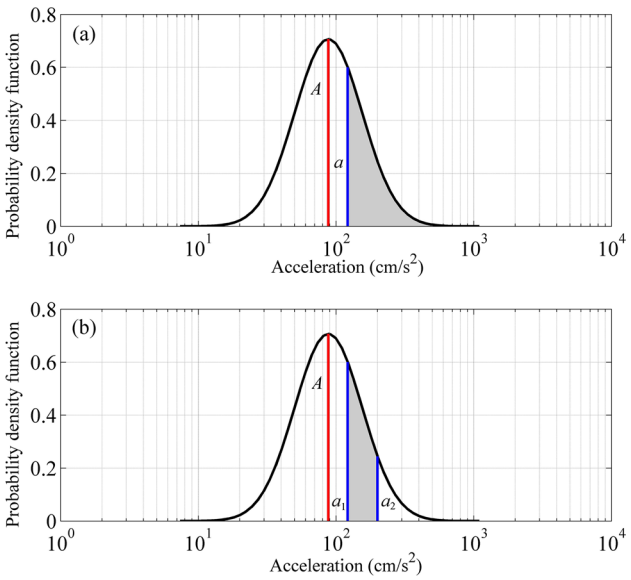

Fig. 5 **a** The probability of ground motion generated by an earthquake exceeding a given value (grey shaded area). **b** The probability of ground motion generated by an earthquake in a certain ground motion interval (grey shaded area). A is the ground motion generated by an earthquake at the site. a is a given ground motion value. $[a_1\ a_2]$ is a given ground motion interval that corresponds to a modified Mercalli intensity (MMI)

in a certain interval (corresponding to an MMI unit), thus able to calculate the annual probability of a given site being affected by an MMI unit:

$$\lambda\,(\mathrm{MMI}) = \sum_i n_i(M_0) \int_{m_0}^{M_u} \int_R P(\mathrm{MMI}|M,\ R) p_i(M) p_i(R) \mathrm{d}R \mathrm{d}M. \tag{6}$$

In the national standard of FGSGMPZMC (General Administration of Quality Supervision, Inspection and Quarantine of the People's Republic of China 2015), the range of PGA ground motion corresponding to intensity VI is 0.04–0.09 g; the range of PGA ground motion corresponding to intensity VII is 0.09–0.19 g; the range of PGA ground motion corresponding to intensity VIII is 0.19–0.38 g; the range of PGA ground motion corresponding to intensity IX is 0.38–0.75 g; and the PGA ground motion greater than or equal to 0.75 g indicate intensity X or above.

6 Results

According to the above-mentioned seismic source model, seismicity parameters, GMMs, and seismic hazard calculation method, the seismic hazards of 118,500 sites in China under 10% and 2% probability of exceedance in 50 years were calculated. In this study, the seismic hazard results for rock site condition were calculated. Users can convert the results of rock sites into the results of site categories of interest according to the conversion coefficients provided by the national standard of Seismic Ground Motion Parameters Zonation Map of China (General Administration of Quality Supervision, Inspection and Quarantine of the People's Republic of China 2015).

The PGA under the generally accepted 10% probability of exceedance in 50 years was chosen for the analysis. Figure 6 is a distribution map of ground motions at 10% probability of exceedance in 50 years. The ground motion values were compared with that calculated by using the FGSSM (Fig. 7). Figure 7 shows that the seismic hazard calculated by the new model increases in certain areas and decreases in others. The areas with increased seismic hazard are mainly distributed in the Tanlu seismic belt, the fault zones around the Ordos block, the Tianshan seismic belt, among other areas. These areas are invariably near the SRAs and fault segments with high hazard coefficient, which is consistent with the parameter allocation principle of the new model. Seismic hazards calculated using the new model have greatly increased due to two factors. First, the increase of seismic rate cited in this study—the data in Table 1 show that the earthquake occurrence rate used in this study has increased by 1 to 2 times in some seismic belts. Second, it is considered in model 3 that all strong earthquakes will occur in SRAs in the next 10 years, which also leads to a significant increase in seismic hazards in these areas. In particular, in the Bohai Bay area, the Beijing–Tianjin–Hebei region, the Yangtze River Delta, and the Guangdong–Hong Kong–Macao Great Bay Area, earthquake hazard is generally on the increase,

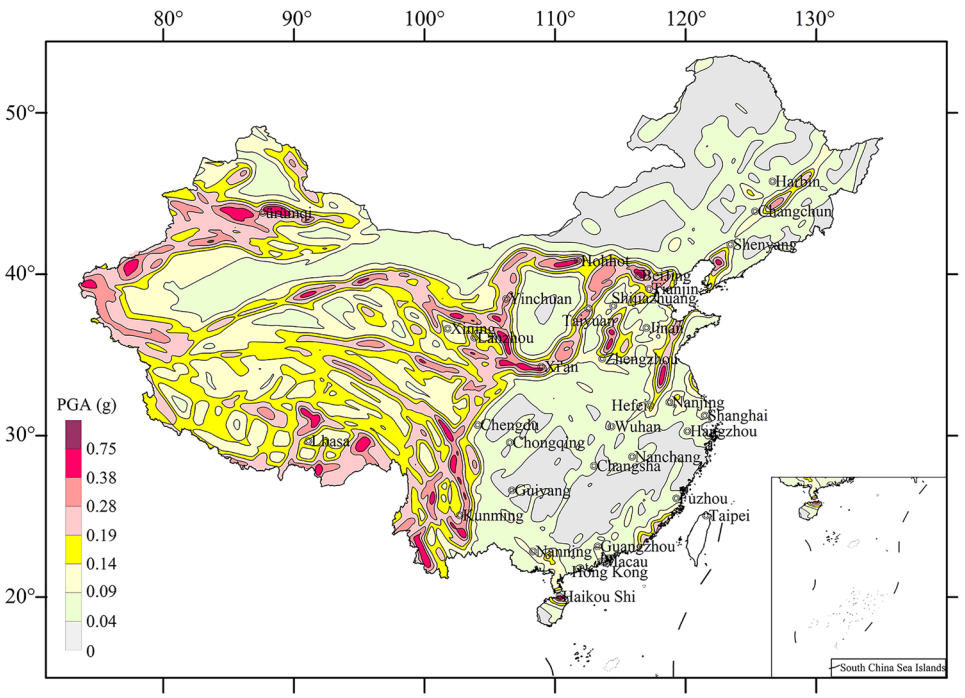

Fig. 6 Peak ground acceleration (PGA) with 10% probability of exceedance in 50 years calculated using the newly built seismicity model in this study

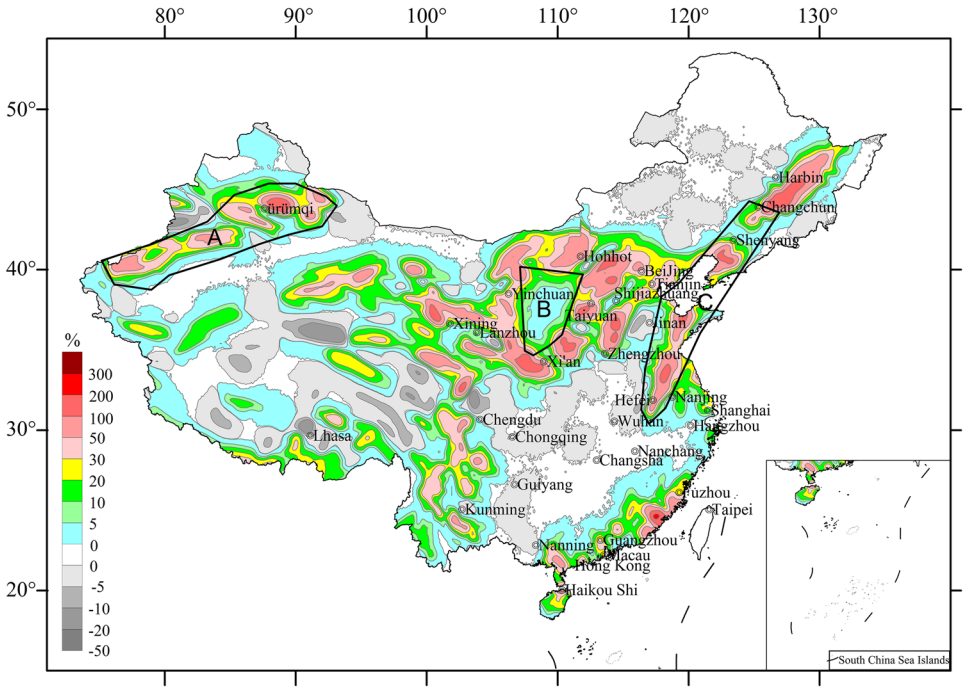

Fig. 7 Comparison of seismic hazards calculated using the new seismicity model with that using the FGSSM ((Results in this study − Result using FGSSM)/Result using FGSSM). The areas with increased seismic hazard are mainly distributed in the Tianshan seismic belt (area A), seismic fault zones around the Ordos block (area B), and the Tanlu seismic belt (area C)

necessitating stronger measures of earthquake prevention and disaster reduction in these areas in the future.

As can be seen in Fig. 7, seismic hazards have decreased in certain areas, such as Northeast China, South China, and the Bayankala block in western China. This is due to the use of the SRA model in this study, which means that in the next 10 years, all major earthquakes will occur in the SRAs, with no major events occurring in other source areas. Therefore, the seismic hazard in areas with no major earthquakes will be lower than that in the fifth generation map.

Figure 8 presents the PGA values amplified by site conditions at 10% and 2% probability of exceedance in 50 years, which we believe will be helpful for other researchers to understand seismic hazard, and help promote relevant prevention and disaster reduction work in China. The classification of site conditions in China's mainland cited in this study was provided by Li et al. (2019).

To predict future earthquake disaster risks, the probability of each site being affected by ground motions at MMI VI, VII, VIII, IX, and ≥X in 2021–2030 was also calculated using Eq. 4 (Figs. 9, 10, 11, 12, 13).

7 Discussion

The hazard results obtained in this study show significant differences when compared to the current fifth generation seismic zonation map of China in certain areas. However, the two are not in conflict, as they serve different purposes. The results in this study represent the seismic hazard level in 2021–2030, while the zonation map represents the average seismic hazard level in the 100 years from 2010 (Pan et al. 2013). The results of the zonation map are mainly used for seismic fortification of general buildings, and the results of this study are mainly used for emergency preparedness. The results of the present study will enable governments at different levels to have a clearer understanding of the seismic hazard areas under their jurisdiction, so as to formulate science-based and reasonable earthquake emergency preparedness policies.

We further compared our calculation results with those of Feng et al. (2020) and Rong et al. (2020). As Feng et al. (2020) used the spatial smoothing method to calculate the seismic hazard of China's mainland with seismic catalogs as main inputs, the spatial distribution characteristics of the calculated results in this study are highly similar to their results in areas with relatively abundant seismic records, such as the Sichuan–Yunnan region. However, the results of Feng et al. (2020) are obviously small in areas where large earthquakes have occurred but with few instrumental seismic records, such as the Tanlu seismic belt. This is because in these areas, seismologists have constructed seismic sources through tectonic analogy and given corresponding seismicity parameters, to ensure that the seismic hazard in these areas is not underestimated (Pan et al. 2013; Zhou et al. 2013).

In this study, the spatial distribution characteristics of seismic hazards under 10% probability of exceedance in 50 years are very similar to those of Rong et al. (2020). For example, areas with relatively high seismic hazard are distributed in large seismic fault zones, such as the Tanlu fault

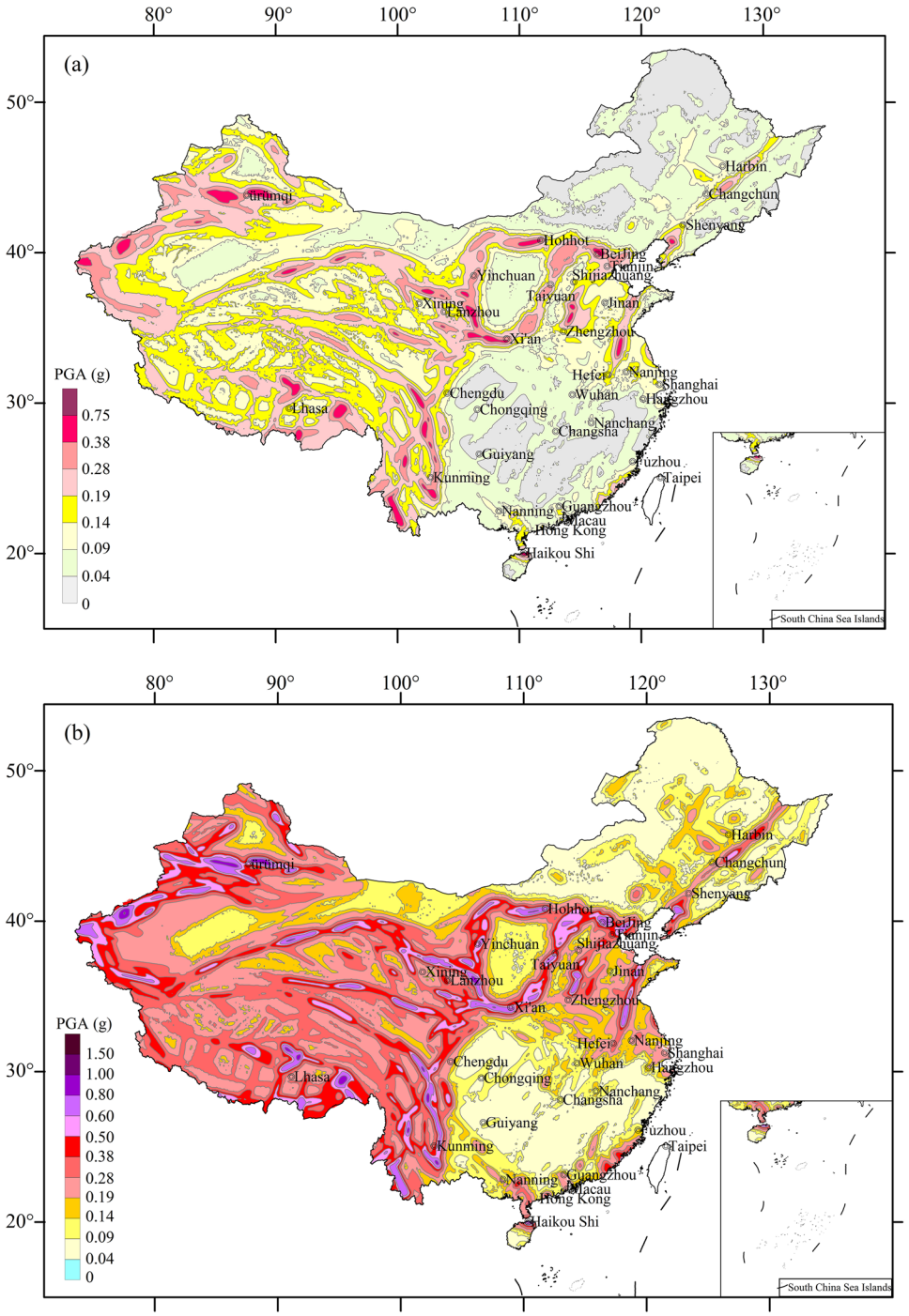

Fig. 8 Peak ground acceleration (PGA) values amplified by site conditions at 10% (**a**) and 2% (**b**) probability of exceedance in 50 years

zone in eastern China, fault zones around the Ordos block in central China, and Xiaojiang fault zone, Xianshuihe fault zone, and Kunlun Mountains fault zone in western China. The areas with lower hazards are also concentrated in Northeast China, South China, the Ordos block, and the Alashan block in western China. This is because some basic data adopted by Rong et al. (2020) are also important basis for the seismic source model division of the fifth generation map adopted in this study. Because the active fault model was given more consideration in Rong et al.'s (2020) work, their results show more spatial details of seismic hazard. In some near-fault areas, their seismic hazard results are higher than those in this study. Because Rong et al. (2020) used the results of geodetic strain rate, their calculated hazard is higher in areas with more active modern seismotectonic movement, such as Xiaojiang fault zone. In addition, differences in the spatial geometry distribution of the seismic source model and the GMM used in this study have also

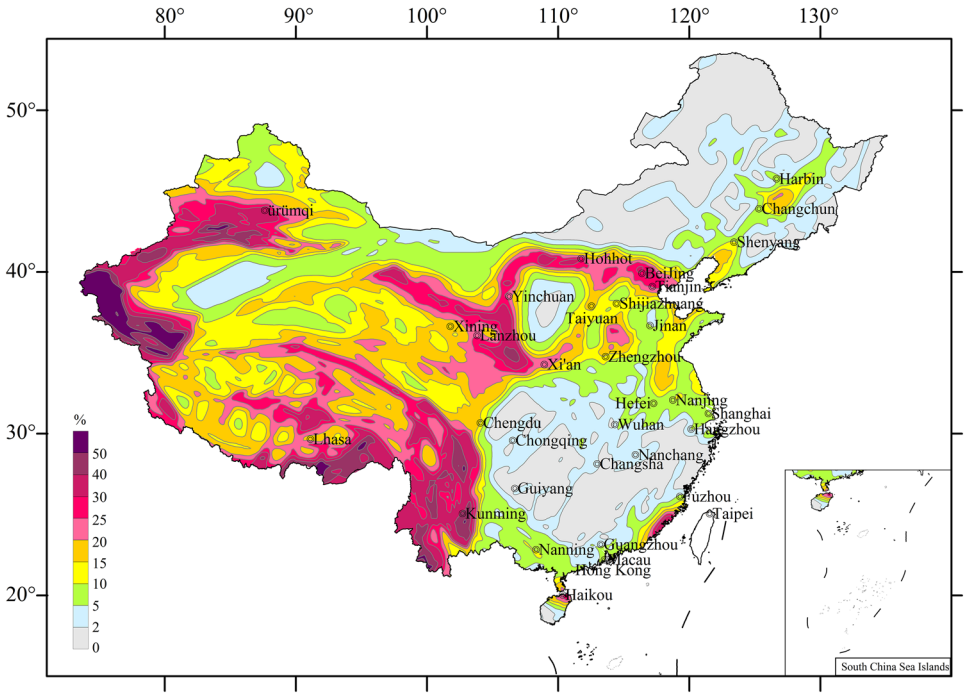

Fig. 9 Spatial distribution of the probability of the modified Mercalli intensity (MMI) VI earthquakes for China's mainland in 2021–2030

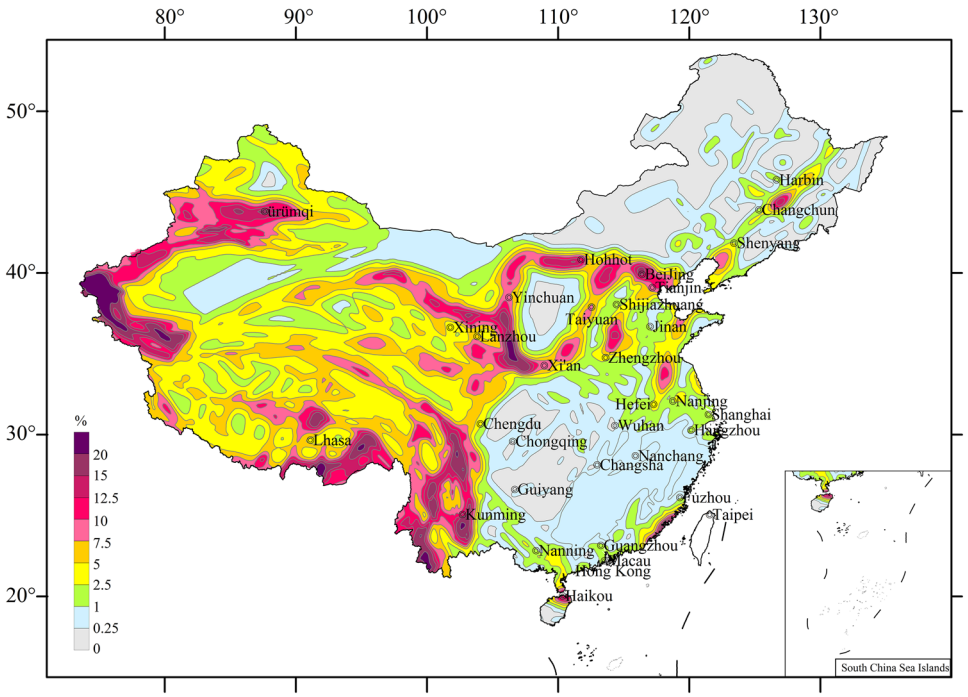

Fig. 10 Spatial distribution of the probability of the modified Mercalli intensity (MMI) VII earthquakes for China's mainland in 2021–2030

contributed to different calculated results from those of Rong et al. (2020).

Through comparisons with the findings of Feng et al. (2020) and Rong et al. (2020), it is clear that regardless of the method and model used, the spatial distribution characteristics of the calculated seismic hazards in China's mainland are generally similar, which are consistent with the seismotectonic structure and seismicity characteristics in the region, in line with the general understanding of seismic hazard in the country. However, due to differences in the geometry of source models, seismicity parameters, and GMMs, the calculated results of specific sites may be different.

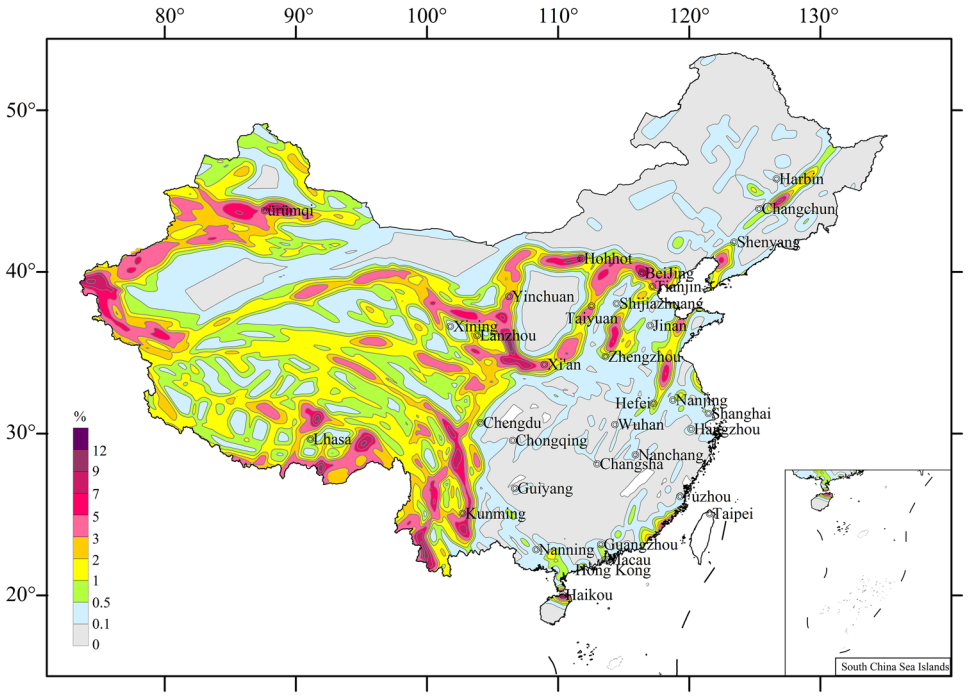

Fig. 11 Spatial distribution of the probability of the modified Mercalli intensity (MMI) VIII earthquakes for China's mainland in 2021–2030

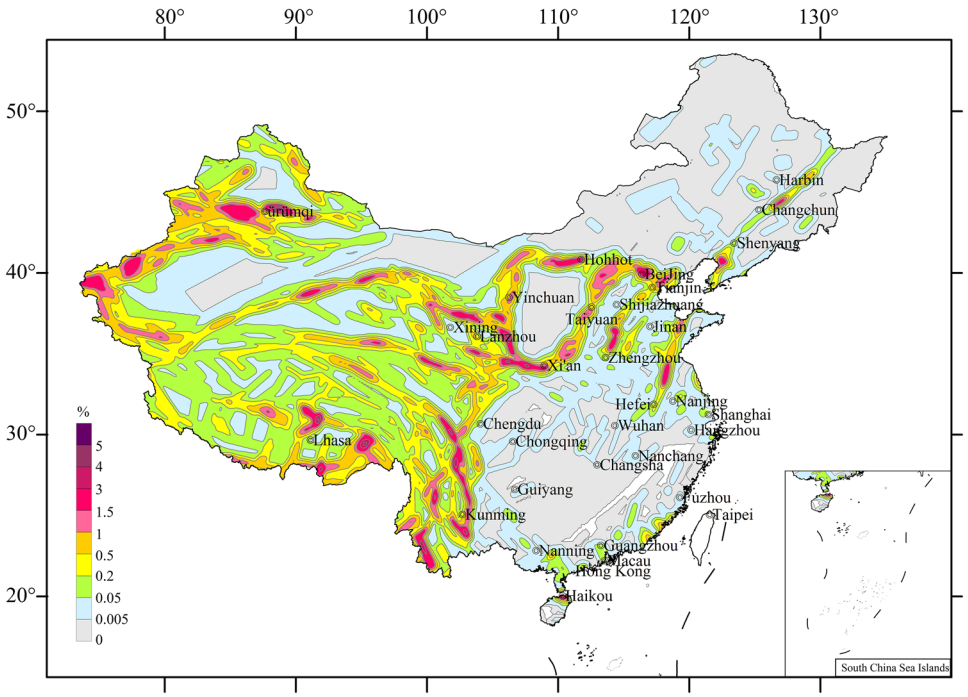

Fig. 12 Spatial distribution of the probability of the modified Mercalli intensity (MMI) IX earthquakes for China's mainland in 2021–2030

In China, with the accumulation of basic data, more quantitative and advanced research methods are now available for estimating the tendency and level of seismicity on individual faults and seismic source zones. For example, Shao et al. (2020) and Shao et al. (2022) provided a quantitative evaluation of the activity level of 391 faults in China in the next 10 years in Northeast China, North China, South China, western China, and the Himalayan arc by using paleoseismic, global positioning system, and geodetic data, and so on. These results have been fully considered in the seismic hazard calculation in this study to update the seismicity model. The new seismicity model reflects the prediction of seismicity levels in 2021–2030 with a scientifically rigorous approach.

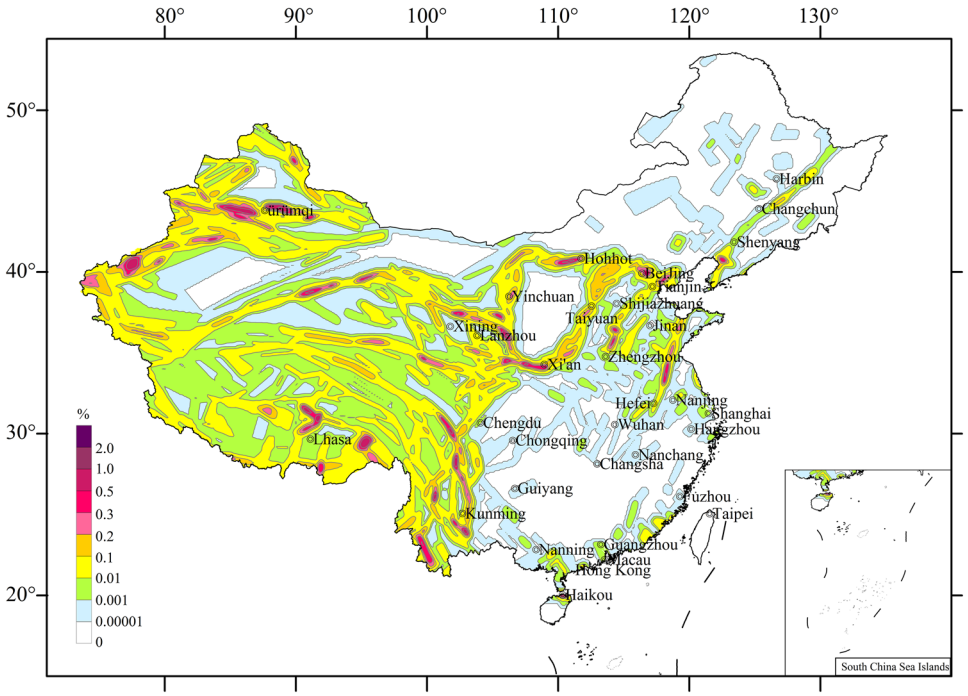

Fig. 13 Spatial distribution of the probability of the modified Mercalli intensity (MMI) greater than or equal to X earthquakes for China's mainland in 2021–2030

8 Conclusion

The merit of the present study lies in the consideration of the spatial and temporal distribution of seismicity in China's mainland in 2021–2030, adopting the occurrence rates of earthquakes in different seismic zones estimated by Shao et al. (2020) and the model of SRAs for the same time period. This holds significance for China's earthquake prevention and disaster reduction work, and may provide a scientific basis for the government's preparation of earthquake emergency relief materials, the reinforcement and reconstruction of key buildings, and the establishment of earthquake insurance models. The calculation results in this study, obtained in general with a scientifically rigorous approach, may be used as input for future seismic risk assessment and serve as a basis for policy making.

Acknowledgments This work was sponsored by the Special Fund of the Institute of Geophysics, China Earthquake Administration (Grant Nos. DQJB22Z03 and DQJB22B25). The authors thankfully acknowledge the constructive suggestions from the two anonymous reviewers. The authors would also like to thank Professor Zhigang Shao and Dr. Peng Wang for their data and constructive suggestions.

References

Bozorgnia, Y., N.A. Abrahamson, L.A. Atik, T.D. Ancheta, G.M. Atkinson, J.W. Baker, A. Baltay, and D.M. Boore et al. 2014. NGA-West2 research project. *Earthquake Spectra* 30(3): 973–987.

CERPG (China Earthquake Risk Prediction Group). 2020. *Forecasting research on earthquake risk area and disaster loss of Chinese mainland during 2016 to 2025*. Beijing: China SinoMaps Press.

Chen, J.G., J.Q. Yan, G.Y. Xu, and Y.Q. Hao. 1999. Discussion on principles and methods in estimating the maximum potential earthquakes in low seismicity area. *Earthquake Research in China* 15(3): 220–228 (in Chinese).

Cornell, C.A. 1968. Engineering seismic risk analysis. *Bulletin of Seismological Society of America* 58(5): 1583–1606.

Cornell, C.A., and E.H. Vanmarck. 1969. The major influences on seismic risk. In *Proceedings of the 4th World Conference on Earthquake Engineering*, 13–18 January 1969, Santiago, Chile.

Cramer, C.H., M.D. Petersen, T.Q. Cao, T.R. Toppozada, and M. Reichle. 2000. A time-dependent probabilistic seismic-hazard model for California. *Bulletin of the Seismological Society of America* 90(1): 1–21.

Deng, Q.D. 1996. Active tectonics in China. *Geological Review* 42(4): 295–299 (in Chinese).

Deng, Q.D., P.Z. Zhang, and Y.K. Ran. 2002. Basic characteristics of active tectonics of China. *Science in China (Series D)* 32(12): 1020–1030 (in Chinese).

Deng, Q.D., P.Z. Zhang, and Y.K. Ran. 2003. Active tectonics and earthquake activities in China. *Earth Science Frontiers* 10(s1): 66–73 (in Chinese).

Feng, C., T.J. Liu, and H.P. Hong. 2020. Seismic hazard assessment for mainland China based on spatially smoothed seismicity. *Journal of Seismology* 24(3): 613–633.

Field, E.H., and T.H. Jordan. 2015. Time-dependent renewal-model probabilities when date of last earthquake is unknown. *Bulletin of Seismological Society of America* 105(1): 459–463.

Frankel, A. 1995. Mapping seismic hazard in the central and eastern United States. *Seismological Research Letters* 66(4): 8–21.

Gao, M.T. 1996. Probability model of earthquake intensity based on Poisson distribution. *Earthquake Research in China* 12(2): 195–201 (in Chinese).

Gao, M.T. 2003. New national seismic zoning map of China. *Acta Seismologica Sinica* 25(6): 630–636 (in Chinese).

Gao, M.T. 2015. *The teaching materials of propaganda and implementation for GB 18306-2015 seismic ground motion parameters zonation map of China*. Beijing: China Standard Press (in Chinese).

Gao, Z.W., G.X. Chen, and B.G. Zhou. 2014. The principles and techniques of identifying seismotectonic province in new national seismic zoning map of China—An example of east China with middle seismic activity. *Technology for Earthquake Disaster Prevention* 9(1): 1–11 (in Chinese).

Gardner, J.K., and L. Knopoff. 1974. Is the sequence of earthquakes in southern California, with aftershocks removed, Poissonian?. *Bulletin of Seismological Society of America* 64(5): 1363–1367.

General Administration of Quality Supervision, Inspection and Quarantine of the People's Republic of China. 2015. *Seismic ground motion parameters zonation map of China (GB18306/2015)*. Beijing: China Standard Press.

Gutenberg, B., and C. Richter. 1944. Frequency of earthquakes in California. *Bulletin of the Seismological Society of America* 34(4): 185–188.

Hong, H.P., and C. Feng. 2019. On the ground-motion models for Chinese seismic hazard mapping. *Bulletin of the Seismological Society of America* 109(5): 2106–2124.

Hu, Y.X., and M.Z. Zhang. 1984. A method of predicting ground motion parameters for regions with poor ground motion data. *Earthquake Engineering and Engineering Vibration* 4(1): 1–11 (in Chinese).

Huan, W.L., W.Q. Huang, X.D. Zhang, and X. Wu. 2002. The division of seismic belts and zones and geodynamic characteristics in China and its adjacent regions. In *Proceedings of the Chinese Geoscience Union*, 440–441. Beijing: Seismological Press (in Chinese).

Li, X.J., B.B. Jing, C. Liu, and J.M. Yin. 2019. Site classification method based on geomorphological and geological characteristics and its application in China. *Bulletin of the Seismological Society of America* 109(5): 1843–1854.

Li, X.J., W.J. Xu, and M.T. Gao. 2022. Probabilistic seismic hazard analysis based on Arias intensity in the north–south seismic belt of China. *Bulletin of the Seismological Society of America* 112(2): 1149–1160.

Lv, Y.J., J. Wang, S.Y. Wang, Y.J. Peng, Z.J. Xie, A.J. Gao, and D.Y. Liu. 2016. *Seismic catalogs for seismic ground motion parameters zonation map of China*. Beijing: Earthquake Press.

Ma, J. 1999. Changing viewpoint from fault to block: A discussion about the role of active block in seismicity. *Earth Science Frontiers* 6(4): 363–370 (in Chinese).

Matthews, M.V., W.L. Ellsworth, and P.A. Reasenberg. 2002. A Brownian model for recurrent earthquakes. *Bulletin of the Seismological Society of America* 92(6): 2233–2250.

Pan, H., M.T. Gao, and F.R. Xie. 2013. The earthquake activity model and seismicity parameters in the new seismic hazard map of China. *Technology for Earthquake Disaster Prevention* 8(1): 11–23 (in Chinese).

Petersen, M.D., T.Q. Cao, K.W. Campbell, and A.D. Frankel. 2007. Time-independent and time-dependent seismic hazard assessment for the State of California: Uniform California earthquake rupture forecast model 1.0. *Seismological Research Letters* 78(1): 99–109.

Petersen, M.D., M.D. Moschetti, P.M. Powers, C.S. Mueller, K.M. Haller, A.D. Frankel, Y.H. Zeng, and S. Rezaeian et al. 2015. The 2014 United States national seismic hazard model. *Earthquake Spectra* 31(1-Suppl): S1–S30.

Rong, Y.F., X.W. Xu, J. Cheng, G.H. Chen, H. Magistrale, and Z.K. Shen. 2020. A probabilistic seismic hazard model for mainland China. *Earthquake Spectra* 36(1-Suppl): 181–209.

Shao, Z.G., G.M. Zhang, and Z.X. Li. 2008. Research on the process and tendency of seismicity along the active tectonic boundaries in Chinese mainland. *Earthquake* 28(3): 33–42 (in Chinese).

Shao, Z.G., Y.Q. Wu, L.Y. Ji, F.Q. Diao, F.Q. Shi, Y.J. Li, F. Long, and H. Zhang et al. 2020. *Determination of key seismic risk areas in Chinese mainland from 2021 to 2030*. Beijing: Institute of Earthquake Prediction, China Earthquake Administration.

Shao, Z.G., Y.Q. Wu, L.Y. Ji, F.Q. Diao, F.Q. Shi, Y.J. Li, F. Long, and H. Zhang et al. 2022. Comprehensive determination for the late stage of the interseismic period of major faults in the boundary zone of active tectonic blocks in Chinese mainland. *Chinese Journal of Geophysics* 65(12): 4643–4658 (in Chinese).

Shao, Z.G., Y.Q. Wu, L.Y. Ji, F.Q. Diao, F.Q. Shi, Y.J. Li, F. Long, and H. Zhang et al. 2023. Assessment of strong earthquake risk in the Chinese mainland from 2021 to 2030. *Earthquake Research Advances* 3(1): Article 100177.

Shi, Z.L., W.L. Huan, X.L. Cao, H.Y. Wu, Y.W. Liu, and W.Q. Huang. 1982. Some characteristics of seismic activity in China. *Chinese Journal of Geophysics* 17(1): 1–13 (in Chinese).

Wang, P., Z.G. Shao, and Q. Liu. 2019. Probabilistic forecasting of earthquakes based on multidisciplinary physical observations and its application in Sichuan and Yunnan. *Chinese Journal of Geophysics* 62(9): 3448–3463 (in Chinese).

Wang, P., Z.G. Shao, X.X. Liu, and X.F. Yin. 2022. Ten-year probability of strong earthquakes on major faults in boundaries of active blocks in Chinese continent. *Chinese Journal of Geophysics* 65(10): 3829–3843 (in Chinese).

Wells, D.L., and K.J. Coppersmith. 1994. New empirical relationships among magnitude rupture length rupture width rupture area and surface displacement. *Bulletin of Seismological Society of America* 84(4): 974–1002.

Wen, X.Z., X.W. Xu, F. Long, and C.F. Xia. 2007. Frequency–magnitude relationship models for assessment of maximum magnitudes of potential earthquakes on moderately and weakly active faults in eastern Chinese mainland. *Seismology and Geology* 29(2): 236–253 (in Chinese).

WGOSHMII (Working Group II on Seismic Hazard Mapping). 2010. *Report on the division of seismic belts and potential seismic sources in China and neighboring regions*. Beijing: Institute of Geophysics, China Earthquake Administration.

Wu, Z.H., Y.Q. Zhang, and D.G. Hu. 2014. Neotectonics active tectonics and earthquake geology. *Geological Bulletin of China* 33(4): 391–402 (in Chinese).

Xiao, L. 2011. Study on attenuation relation of strong ground motion parameters of horizontal bedrock. Ph.D. Dissertation. Institute of Geophysics, China Earthquake Administration, Beijing, China.

Xie, F.R., S.M. Zhang, Y.Q. Zhang, J.J. Ren, X.L. Zhang, and H.L. Ran. 2013. Recurrence interval of large earthquakes along Chinese mainland active fault. *Technology for Earthquake Disaster Prevention* 8(2): 1–10 (in Chinese).

Xu, W.J., M.T. Gao, and H.Q. Zuo. 2021. Generation of a stochastic seismic event set based on a new seismicity model in China's earthquake catastrophe model. *Seismological Research Letters* 92(4): 2308–2320.

Yu, Y.X., S.Y. Li, and L. Xiao. 2013. Development of ground motion attenuation relations for the new seismic hazard maps of China. *Technology for Earthquake Disaster Prevention* 8(1): 24–33 (in Chinese).

Zhang, P.Z. 1999. Late quaternary tectonic deformation and earthquake hazard in continental China. *Quaternary Sciences* 39(5): 404–413 (in Chinese).

Zhang, P.Z., Q.D. Deng, G.M. Zhang, J. Ma, W.J. Gan, W. Min, F.Y. Mao, and Q. Wang. 2003. Active tectonic blocks and strong earthquakes in the continent of China. *Science in China (Series D)* 33(s1): 12–20 (in Chinese).

Zhang, G.M., H.S. Ma, H. Wang, and L. Li. 2004. Relationship between the active blocks in Chinese mainland and the strong seismic activity. *Science in China (Series D)* 34(7): 591–599 (in Chinese).

Zhang, P.Z., Q.D. Deng, Z.Q. Zhang, and H.B. Li. 2013. Active faults, earthquake hazards and associated geodynamic processes in continental China. *Science in China (Series D)* 43(10): 1607–1620 (in Chinese).

Zheng, W.J., P.Z. Zhang, D.Y. Yuan, C.Y. Wu, Z.G. Li, W.P. Ge, W.T. Wang, and Y. Wang. 2019. Basic characteristics of active tectonics and associated geodynamic processes in continental China. *Journal of Geomechanics* 25(5): 699–721.

Zhou, B.G., H.L. Ran, X.C. Song, and Q. Zhou. 2003. An inhomogeneous distribution model of strong earthquakes along strike-slip active fault segments on the Chinese continent and its implication in engineering seismology. *Earthquake Research in China* 19(3): 101–111 (in Chinese).

Zhou, B.G., G.X. Chen, and Z.W. Gao. 2013. The technical highlights in identifying the potential seismic sources for the update of national seismic zoning map of China. *Technology for Earthquake Disaster Prevention* 8(2): 113–124 (in Chinese).

Zöller, G. 2018. A statistical model for earthquake recurrence based on the assimilation of paleoseismicity, historic seismicity, and instrumental seismicity. *Journal of Geophysical Research: Solid Earth* 123: 4906–4921.